Progress In Electromagnetics Research C, Vol. 12, 27–36, 2010

DEVELOPMENT OF AN ELLIPTICAL ANNULAR RING MICROSTRIP ANTENNA WITH SINE WAVE PERIPHERY

M. Baharuddin†, V. Wissan, J. T. Sri Sumantyo, and H. Kuze

Microwave Remote Sensing Laboratory
Center for Environmental Remote Sensing
Chiba University
1-33 Yayoi-cho, Inage-ku, Chiba-shi 263-8522, Japan

Abstract—We have investigated elliptical annular ring microstrip antennas having a sine wave periphery both theoretically and experimentally. The proposed antenna gives a good circular polarization at the center frequency of 1.285 GHz, with measured 3 dB axial ratio bandwidth of about 0.73% (9.5 MHz) and impedance bandwidth of about 1.7% (22.0 MHz). Input and radiation characteristics are also examined for different sine wave amplitudes applied to the periphery of elliptical ring patch antenna.

1. INTRODUCTION

Circularly-polarized (CP) microstrip antennas have been developed with both dual- and single-feed architecture. Single-feed CP microstrip antennas [1–6] are more compact as compared to the dual-feed ones. One of the single feed CP microstrip antennas is elliptical annular ring microstrip antenna that produces circularly polarized wave of very good quality [6].

In this paper, we propose a single-feed, circularly-polarized, elliptical annular-ring microstrip antenna (EARMA) operated in the L-band (1.285 GHz). The antenna periphery is modulated with a sinusoidal wave, giving a flowery appearance. An annular ring microstrip antenna (ARMA) with a periodically added sector stubs at the outer and inner edgez has been reported [7] to have a relatively wider bandwidth and smaller size than ordinary ARMAs. Fractal

Corresponding author: M. Baharuddin (merna5@graduate.chiba-u.jp).
† Also with Faculty of Engineering, Department of Electrical Engineering, Hasanuddin University, Jalan Perintis Kemerdekaan Km.10 Makassar, Indonesia.

geometry applied to the periphery of microstrip antennas has also led to the reduction of the antenna size and broadening of the bandwidth [8–10]. Therefore, it is expected that by applying sine wave pattern to the periphery of the EARMA, broader bandwidth and reduced antenna size will be obtained. In this work, the characteristics of such antennas are investigated by both simulation and experiment. It turns out that favorable characteristics of input parameter and radiation pattern in broadside direction can be achieved, ensuring its application to circularly-polarized L-band applications such as global positioning system (GPS), synthetic aperture radar (SAR), television broadcasting, etc.

2. ANTENNA PARAMETER

Circular polarization is produced from the EARMA by locating the feed point of the antenna element on the radial line that is rotated 45° counterclockwise (or clockwise) to the semi major-axis of the ellipse for a left-handed (or right-handed) circularly-polarized (LHCP/RHCP) radiation. We adopt the proximity-coupled feeding method that has the advantage of easier adjustment in the design and fabrication processes, especially in producing good circular polarization with good impedance matching.

The configuration of the radiating element, together with the microstrip line feed and ground plane, is shown in Fig. 1(a), where important parameters are labeled. The periphery (outer ring) is an ellipse modulated with a sine wave, and in the Cartesian coordinate system, it can be expressed as

$$\frac{x^2}{\left[a + m\sin 8\left(\tan^{-1}\frac{y}{x}\right)\right]^2} + \frac{y^2}{\left[b + m\sin 8\left(\tan^{-1}\frac{y}{x}\right)\right]^2} = 1,$$

Table 1. Geometry parameters (in units of mm) of EARMA models 1-3.

	a	b	a_1	b_1	d	w	l	l_s	w_s	l_a	l_r
Antenna-1 ($m = 3$)	42.4	41.1	9.85	8.9	15.3	3.0	43.1	6.0	7.0	130.0	129.4
Antenna-2 ($m = 5$)	41.5	40.3	9.85	8.9	19.8	3.0	45.1	6.0	7.0	120.0	130.9
Antenna-3 ($m = 9$)	36.8	35.9	9.85	8.9	18.8	3.0	72.1	6.0	7.0	120.0	156.9

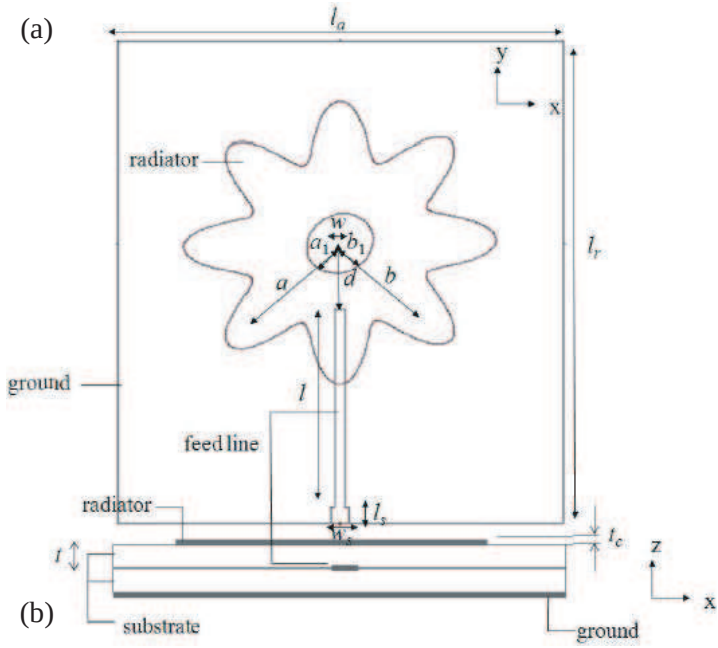

Figure 1. Configuration of the elliptical annular ring microstrip antenna (EARMA) with proximity coupled feed; (a) top view and (b) side view.

where m is the amplitude of the sine wave, and a and b are the semi-major and -minor axes of the outer elliptical ring, respectively. The inner ellipse is given by the ordinary ellipse equation:

$$\frac{x^2}{a_1^2} + \frac{y^2}{b_1^2} = 1$$

where a_1 and b_1 are the semi-major and -minor axes of the inner elliptical ring, respectively.

Three different cases are considered here in terms of the m parameter, while the working frequency concerning the axial ratio (AR) is 1.285 GHz for all cases. Table 1 shows the dimensions of the radiator, microstrip line feed, and the ground plane for the EARMA patch models assumed in the simulation study. Side view is depicted in Fig. 1(b). The geometry model is implemented on two substrates, each with thickness $t = 1.6$ mm, conductor thickness $t_c \approx 0.035$ mm, relative permittivity $\varepsilon_r = 2.17$ and dissipation factor 0.0005. With the width of the microstrip line of 3 mm, the characteristic impedance is approximately 68.3 Ω.

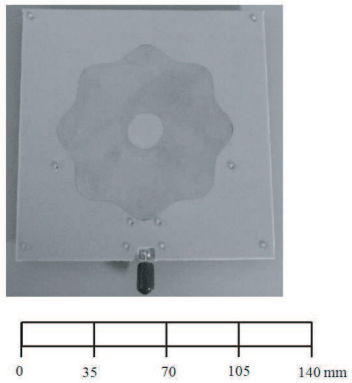

Figure 2. Fabricated EARMA patch with sine wave periphery (Antenna-1, $m = 3$).

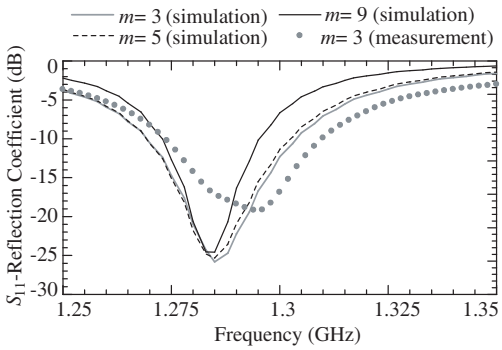

Figure 3. Frequency dependence of simulated and measured reflection coefficient.

The EARMA radiator will generate LHCP by rotating the patch by $-45°$ around the center of the patch. Simulations with a finite-ground-plane model have been undertaken to optimize the size parameters using a full-wave analysis tool (IE3D Zeland software) based on the method of moment (MoM) algorithm. Although all three models ($m = 3$, 5, and 9) are investigated in the simulation study, one EARMA patch having $m = 3$ is actually fabricated and tested. In the following section, the simulation results for all antenna model and measurement results for the case of $m = 3$ (Antenna-1) will be described.

3. RESULTS AND DISCUSSION

Figure 2 shows the picture of the EARMA patch, based on the parameters of Antenna-1 ($m = 3$) given in Table 1. Fig. 3 shows the frequency dependence of the S_{11}-parameter (reflection coefficient) obtained from the simulation (for Antenna-1 to -3) and measurement (Antenna-1). A gradual shift toward lower frequency is seen at the lowest value of S_{11}-parameter as the value of m is increased in the simulation. Decrease in the impedance bandwidth is observed with the increased value of m: the bandwidth ($S_{11} < -10\,\text{dB}$) is 34, 33 and 23 MHz (2.7, 2.6, and 1.8%) for $m = 3$, 5 and 9, respectively. Fig. 3 also shows that experimentally, the reflection coefficient of Antenna-1 takes a minimum value at $f_1 = 1.295\,\text{GHz}$. This frequency

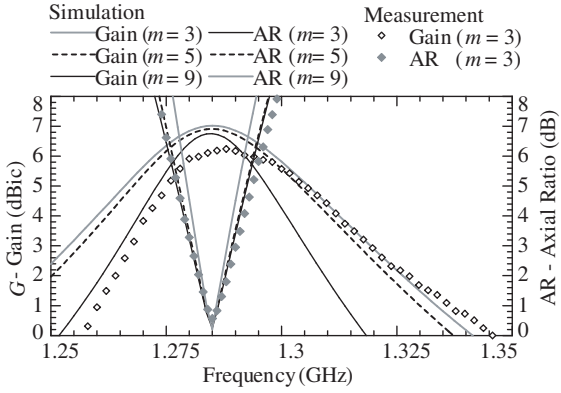

Figure 4. Frequency dependence of simulated and measured gain and AR at θ angle $= 0°$.

is somewhat higher than the operation frequency of $f_0 = 1.285$ GHz, though an impedance bandwidth ($S_{11} < -10$ dB) of more than 30 MHz is attained around f_1. Such a difference between the simulated and experimental results (seen also in other curves in Figs. 4 and 6 shown below) can probably be ascribed to the fabrication imperfections (such as inaccuracy in the milling and etching processes, connector soldering and holes with plastic screws) and/or the substrate loss and cable loss.

In Fig. 4, the antenna gain and AR at θ angle $= 0°$ are plotted against the frequency. The gain of the antenna is simulated to be around 7.0, 6.9 and 6.7 dBic for Antenna-1, -2 and -3 at 1.285 GHz, respectively. As for the frequency dependence curves of AR, a crucial parameter for circularly-polarized antenna operation, the values of 3-dB AR bandwidth simulated for Antenna-1 through Antenna-3, are 9.01, 8.56, and 6.56 MHz (0.70, 0.66, and 0.51%) respectively. From the measurement of Antenna-1, on the other hand, the gain is obtained to be 6.1 dBic, to some extent smaller than the simulated value of 7.0 dBic at 1.285 GHz. The measured 3-dB AR bandwidth is 9.5 MHz, slightly wider than the simulated result. All the models exhibit narrower bandwidths than the ordinary EARMA model simulated at the same working frequency (40.2 MHz or 3.1% of -10 dB S_{11} bandwidth and 9.8 MHz or 0.76% of 3-dB AR bandwidth).

Vector current distributions simulated for Antenna-1 through Antenna-3 are shown in Fig. 5. Stronger distributions (larger vectors) are concentrated at the edge of the inner ring, at some of the dips along the sine-wave periphery and some areas between them. The size of the vector is related to the current intensity on the surface of the antenna.

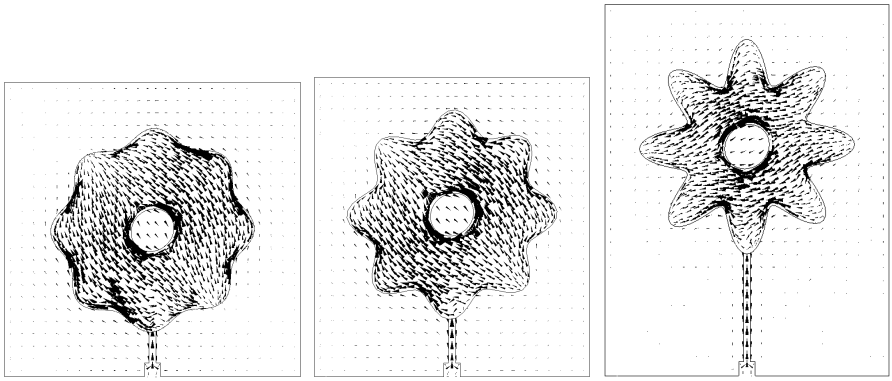

Figure 5. Vector current distribution of (a) Antenna-1, (b) Antenna-2, and (c) Antenna-3 at 1.285 GHz.

Most of the smaller-sized vectors appear at some peak areas of the outer peripheral ring. The results in Fig. 5 indicate that the larger is the value of m, the narrower is the area that contains larger-sized vectors. Presumably this is the cause of the narrower impedance, gain and AR bandwidths associated with antenna models having larger m values.

The EARMAs' size (in terms of the rectangular area covering the radiator region) is not reduced (see parameters a and b, total with the m value in Table 1) compared with the ordinary EARMA ($a = 43.2\,\text{mm}$; $b = 41.9\,\text{mm}$). However, the radiator areas are reduced. The radiator areas of Antenna-1, -2, and -3 are 5198.6, 5001.3, and 3982.1 mm^2, respectively. Since the radiator area of an ordinary EARMA with the same working frequency is simulated to be 5386.6 mm^2, all EARMAs have achieved radiator size reduction.

Average current distributions of the microstrip line feed for Antenna-1 through Antenna-3 are shown in Fig. 6. This figure shows the distribution of surface current intensity which is varied along with the microstrip line length. The brighter the regions, the stronger the surface current intensity is. The microstrip line feed should be longer for the larger value of m (see also Table 1 and Fig. 5) even though they have the same electrical length of 90°. This is presumably due to the longer surface current path with a larger value of m. The widest bending geometry (with most meandered surface current path) found in Antenna-3 has resulted in the increase in electrical length and hence the decrease in the overall antenna surface area for the same working frequency.

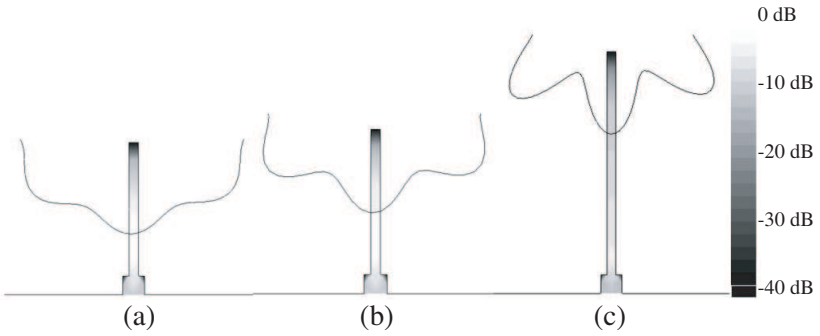

Figure 6. Average current distribution of the microstrip line feed of (a) Antenna-1, (b) Antenna-2, and (c) Antenna-3 at 1.285 GHz.

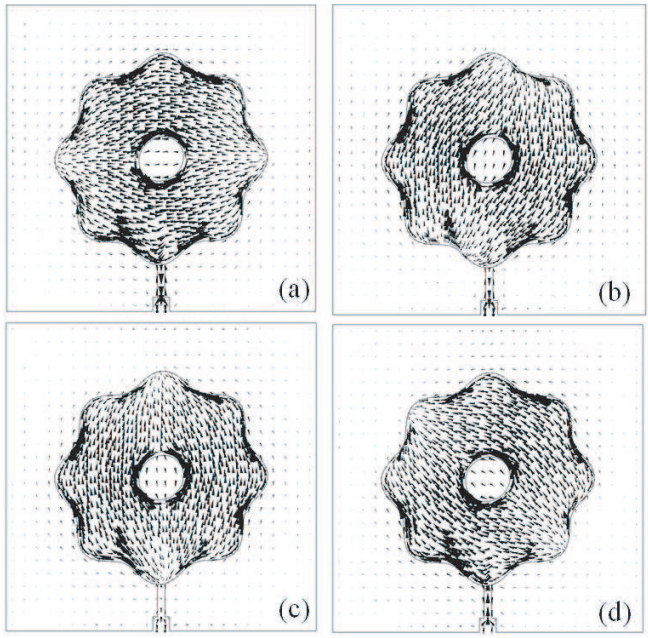

Figure 7. Vector current distribution of Antenna-1 at ϕ angle (a) 0°, (b) 45°, (c) 90°, and (d) 135°.

Figure 7 shows the vector current distribution of Antenna-1 in which the strongest distribution is located at the azimuth angle $\phi = 0°$, 45°, 90°, and 135° respectively. From this figure it can be inferred that the antenna is a left-handed circular polarization (LHCP) antenna, as the vector current rotating clockwise.

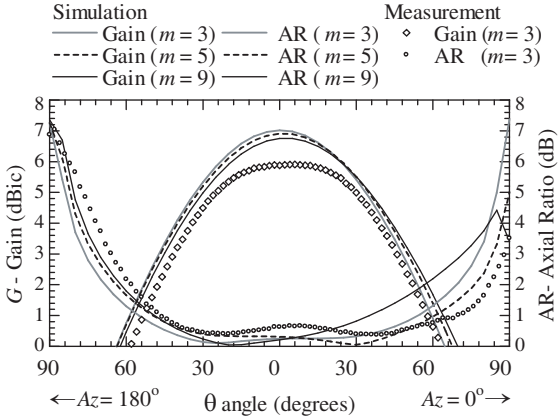

Figure 8. Simulated and measured gain and AR vs. theta angle (radiation pattern) in the theta plane ($Az = 0°$ and 180°) (x-z plane) at $f = 1.285$ GHz.

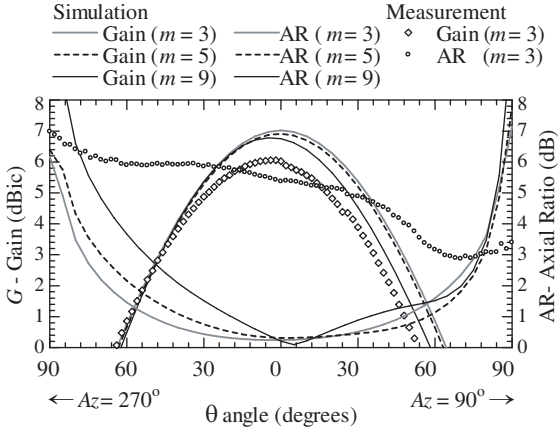

Figure 9. Simulated and measured gain and AR vs. theta angle (radiation pattern) in the theta plane ($Az = 90°$ and 270°) (y-z plane) at $f = 1.285$ GHz.

Spatial distributions (radiation pattern) of the gain and AR at an azimuth angle $Az = 0°$ (and 180°, x-z plane) and $Az = 90°$ (and 270°, y-z plane) are shown in Figs. 8 and 9, respectively, both at the frequency of $f = 1.285$ GHz. From the simulation at the azimuth angle $Az = 0°$, the 5-dBic gain beamwidth is 60° for Antenna-1/2 and 55° for Antenna-3, while the beamwidths for the 3-dB AR are 150° for Antenna-1/2 and 140° for Antenna-3. The measurement at the

azimuth angle $Az = 0°$ shows the 5-dBic gain beamwidth of 53° and 3-dB AR beamwidth of 152°. At the $Az = 90°$, the simulated 5-dBic gain beamwidth is 60° for Antenna-1/2 and 55° for Antenna-3, while the beamwidths for the 3-dB AR are 150° for Antenna-1/2 and 140° for Antenna-3. The measured antenna shows a 5-dBic gain beamwidth of 46° at $Az = 90°$. At this plane also, measured AR characteristic shows higher value than 3 dB at the whole 180° range. This particular AR measurement result is probably attributed by the difference in geometry antenna size (between simulated and fabricated model for adjustment) due to the substrate variation. The very sensitive AR characteristic may be improved in the future by further adjustment in fabrication process.

Except for the $Az = 90°$ AR characteristics, there are slight differences in beamwidth of 5-dBic gain and 3-dB AR as compared with the simulated model which is probably due to the imperfections mentioned above.

4. CONCLUSION

A new annular ring microstrip antenna with elliptical shape modulated with sine wave has been presented. Numerical analysis and measurement results have shown that this antenna has good circular polarization characteristics over a bandwidth of around 9 MHz and fairly high gain at the observed operation frequency of 1.285 GHz. Further enhancement of the 3-dB AR bandwidth and reduction of the antenna size can probably be achieved using advanced techniques depending on the application requirement. Simulation studies have also been undertaken with respect to the effects of the sine wave amplitude on the antenna performance. With its good performance, this novel antenna patch will be useful for circularly-polarized L-band applications such as GPS, synthetic aperture radar, and television broadcasting.

ACKNOWLEDGMENT

The authors would like to thank Basari, Muhammad Fauzan, Prilando R. A., Yohandri and Iman for assisting in the antenna fabrication and measurement; the Japan Society for the Promotion of Science (JSPS) for Grant-in-Aid for Scientific Research-Young Scientist (A) (No. 19686025); National Institute of Information and Communication Technology (NICT) for International Research Collaboration Research Grant 2008, Chiba University COE Start-up Program, European Space Agency (ESA) Earth Observation Category 1 (No. 6613), the

research grant for Mission Research on Sustainable Humanosphere from Research Institute for Sustainable Humanosphere (RISH), Kyoto University and other research grants that have supported this research.

REFERENCES

1. Yang, S. S., K.-F. Lee, A. A. Kishk, and K.-M. Luk, "Design and study of wideband single feed circularly polarized microstrip antennas," *Progress In Electromagnetics Research*, PIER 80, 45–61, 2008.
2. Sharma, P. and K. Gupta, "Analysis and optimized design of single feed circularly polarized microstrip antennas," *IEEE Trans. Antennas Propag.*, Vol. 31, No. 6, 949–955, 1983.
3. Nasimuddin, K. P. Esselle, and A. K. Verma, "Wideband circularly polarized stacked microstrip antennas," *IEEE Antennas and Wireless Propagation Letters*, Vol. 6, 21–24, 2007.
4. Kan, H. K. and R. B. Waterhouse, "Low cross-polarised patch antenna with single feed," *IEEE Electronic Letters*, Vol. 43, No. 5, 9–10, 2007.
5. Row, J.-S. and C.-Y. Ai, "Compact design of single-feed circularly polarised microstrip antenna," *IEEE Electronic Letters*, Vol. 40, No. 18, 1093–1094, 2004.
6. Bhattacharyya, A. K., "Theoretical and experimental investigation of the elliptical annular ring antenna," *IEEE Trans. Antennas Propag.*, Vol. 36, No. 11, 1526–1530, 1988.
7. Hong, W., C.-T. Cheng, Y.-D. Lin, and T. Kitazawa, "A novel dual circularly polarized microstrip antenna," *36th European Microwave Conference*, 1629–1632, 2006.
8. Gianvittorio, J. and Y. Rahmat-Samii, "Fractal antennas: A novel antenna miniaturization technique, and applications," *IEEE Antennas Propagation Mag.*, Vol. 44, 20–36, 2002.
9. Krishna, D. D., M. Gopikrishna, C. K. Aanandan, P. Mohanan, and K. Vasudevan, "Compact wideband Koch fractal printed slot antenna," *IET Microwaves, Antennas & Propagation*, Vol. 3, No. 5, 782–789, 2009.
10. Chen, W.-L., G.-M. Wang, and C.-X. Zhang, "Bandwidth enhancement of a microstrip-line-fed printed wide-slot antenna with a fractal-shaped slot," *IEEE Trans. Antennas Propag.*, Vol. 57, No. 7, 2176–2179, 2009.